

Mapping of erosion rates in marly badlands based on a coupling of anatomical changes in exposed roots with slope maps derived from LiDAR data

Jérôme Lopez Saez,^{1*} Christophe Corona,¹ Markus Stoffel,^{2,3} Georges Rovéra,⁴ Laurent Astrade⁵ and Frédéric Berger¹

¹ Cemagref UR EMGR, Saint-Martin d'Hères, France

² Laboratory of Dendrogeomorphology (dendrolab.ch), Institute of Geological Sciences, University of Bern, Bern, Switzerland

³ Climatic Change and Climate Impacts, Institute for Environmental Sciences, University of Geneva, Carouge-Geneva, Switzerland

⁴ Institut de Géographie Alpine, Université Joseph Fourier, Grenoble, France

⁵ Université de Savoie - CISM, Laboratoire EDYTEM, Le Bourget du Lac, France

Received 3 August 2010; Revised 25 January 2011; Accepted 25 January 2011

*Correspondence to: Jérôme Lopez Saez, Cemagref UR EMGR, 2 rue de la papeterie, BP 76 F-38402 Saint-Martin d'Hères Cedex, France.
E-mail: jerome.lopez@cemagref.fr

ESPL

Earth Surface Processes and Landforms

ABSTRACT: Black marls form very extensive outcrops in the Alps and constitute some of the most eroded terrains, thus causing major problems of sedimentation in artificial storage systems (e.g. reservoirs) and river systems. In the experimental catchments near Draix (France), soil erosion rates have been measured in the past at the plot scale through a detailed monitoring of surface elevation changes and at the catchment scale through continuous monitoring of sediment yield in traps at basin outlets. More recently, erosion rates have been determined by means of dendrogeomorphic techniques in three monitored catchments of the Draix basin. A total of 48 exposed roots of Scots pine have been sampled and anatomical variations in annual growth rings resulting from denudation analysed. At the plot scale, average medium-term soil erosion rates derived from exposed roots vary between 1.8 and 13.8 mm yr⁻¹ (average: 5.9 mm yr⁻¹) and values are significantly correlated with slope angle. The dendrogeomorphic record of point-scale soil erosion rates matches very well with soil erosion rates measured in the Draix basins. Based on the point-scale measurements and dendrogeomorphic results obtained at the point scale, a linear regression model involving slope angle was derived and coupled to high-resolution slope maps obtained from a LiDAR-generated digital elevation model so as to generate high-resolution soil erosion maps. The resulting regression model is statistically significant and average soil erosion rates obtained from the areal erosion map (5.8, 5.2 and 6.2 mm yr⁻¹ for the Roubine, Moulin and Laval catchments, respectively) prove to be well in concert with average annual erosion rates measured in traps at the outlet of these catchments since 1985 (6.3, 4.1 and 6.4 mm yr⁻¹). This contribution demonstrates that dendrogeomorphic analyses of roots clearly have significant potential and that they are a powerful tool for the quantification and mapping of soil erosion rates in areas where measurements of past erosion is lacking. Copyright © 2011 John Wiley & Sons, Ltd.

KEYWORDS: roots; dendrogeomorphology; marly badlands; erosion rates; LiDAR; mapping

Introduction

Marly lithologies are well known for their high vulnerability to erosion processes, particularly in the Mediterranean environments of Spain (e.g. Sirvent *et al.*, 1997; Bouma and Imeson, 2000), Italy (e.g. Clarke and Rendell, 2010), Morocco (e.g. Tribak *et al.*, 2009), and Israel (e.g. Kuhn and Yair, 2004). In the Durance basin located in the southern French Alps, erosion in marly badlands is enhanced by the nature of the Mediterranean climate (Lasanta *et al.*, 2001), the sparse vegetation cover and highly erodible lithology (Descroix and Olivry, 2002), resulting in erosion rates of up to 10 mm yr⁻¹ (Walling, 1988; Delannoy and Rovéra, 1996). One of the consequences of enhanced erosion is high sediment yield at the outlet of catchments (Mathys *et al.*, 2003; Mathys and Poesen, 2005) and an increased silting of reservoirs (Verstraeten *et al.*, 2006). This silting results in a considerable deterioration of all functions of

storage lakes (such as hydro-electricity, irrigation) and, consequently, in reduced useful lifetimes of dams. Furthermore, high sediment yields can have severe impacts on the fluvial ecosystems (Verstraeten *et al.*, 2006). A large number of erosion studies has been carried out in the Durance basin to quantify sediment yield and the effect of restoration strategies (see Descroix and Mathys, 2003, for a detailed review). Methodological devices used for the measurement of soil losses can be divided into two groups: those that measure soil loss *in situ* and those that quantify erosion at the outlet of a plot or a catchment (Descroix and Mathys, 2003). As an alternative to these traditional methods, temporally and spatially distributed data may also be inferred from the identification and analyses of bio-markers such as dendrogeomorphic techniques (Stoffel *et al.*, 2010) so as to expand the series of quantitative data to decadal or even centennial time scales. Exposed roots have been used in dendrogeomorphology since the 1960s

(Stoffel and Bollschweiler, 2008) and erosion rates were directly inferred from (i) the position of the root axis, considered as a fixed spatial reference relative to the current ground surface; (ii) the year of exposure determined through the study of changes in the ring-growth pattern (e.g. LaMarche, 1968) and, more recently, in the anatomical structure of the root (e.g. Corona *et al.*, 2011).

In this study, multi-decadal erosion rates at the plot scale were obtained from exposed Scots pine (*Pinus sylvestris* L.) roots. They were coupled with highly-resolved terrain information in the Draix experimental catchments. The objectives were: (i) to create quantitative areal erosion maps based on dendrogeomorphic results; (ii) to evaluate the representativeness, reliability and accuracy of these measurements at the catchment scale through a comparison of reconstructed erosion rates with trap sedimentation data gathered at the outlet of the basins.

Study Site

Fieldwork was carried out in the Draix experimental catchment basins (Figure 1a) located in the southern French Alps near the town of Digne-les-Bains (44°08'N, 6°20'E) where four basins have been monitored continuously since 1982 and where data exists on rainfall, liquid discharge, solid transport and sediment yield at the basins' outlet. The four basins have different surface areas ranging from 0.13 to 100 ha (Table I). Three of the sites (i.e. Roubine, Moulin and Laval catchments) are situated in denuded areas with vegetation cover ranging from 21% to 56%. The fourth site (Brusquet) has not been analysed in the present study as it has been reforested at the end of the nineteenth century within the frame of restoration works and therefore has 87% of its surface area covered with *Pinus sylvestris*. The basins analysed are developed on Jurassic marine black marls belonging to Bajocian, Bathonian and Callovo-Oxfordian units and are characterized by dense layering. These formations are capped by fairly resistant limestone lithologies controlling topography and forming elongated monoclinical ridges with elevations reaching up to 2000 m above sea level (a.s.l.) (Oostwoud Wijdenes and Ergenzinger, 1998). The marly formations at Draix are very sensitive to weathering and erosion (Antoine *et al.*, 1995) which has resulted in characteristic badlands morphology with V-shaped gullies.

The Roubine basin (0.13 ha) is dominated by a steep gully with slope gradients in the main channel >35%; it can be considered an elementary unit to observe erosion phenomena. The Moulin basin (8 ha) is an intermediate scale basin with a small channel network and a length of the main channel of 300 m. The Laval basin (86 ha) is composed of several sub-catchments draining into a main channel about 1 km in length.

Climate in the region is of the Mediterranean type with mean annual rainfall (1984–2004) of 900 mm, an average of 200 days without rain and only five days with rainfall depths >30 mm. Summers are generally dry with occasional storms. Precipitation maxima and runoff peaks occur in spring (April–May) and autumn (September–October, Richard and Mathys, 1999). Mean annual temperature is 9.8°C with warm summers (+28°C in July) and mild winters but an average of 115 freeze–thaw cycles has been recorded during experiments between November and April (Rovéra and Robert, 2005). Snow is not unusual but does not form a semi-permanent cover.

Local studies on weathering processes and regolith dynamics show that the alternation of freeze–thaw and wetting–drying cycles represents the main triggers of regolith development and weathering (Antoine *et al.*, 1995) in the Durance basin. The

actual evolution of badland surfaces is clearly related to regolith moisture and temperature and differs between seasons and slope exposure, thus resulting in cyclical variations in physical regolith conditions. At the end of each winter, a loose detrital layer of locally produced clasts or colluvial material, 5–10 cm in thickness, usually covers the fragmented regolith (10–50 cm) laying on the marly bedrock (Maquaire *et al.*, 2002) and rills formed in the previous year have mostly disappeared. In the absence of runoff in winter, marl platelets will have fallen due to gravity and frost creep and accumulated at the bottom of the slopes, ready to be eroded by the first runoff event (Rovéra *et al.*, 1999). In addition, saturation of the weathered layer by melting snow may cause solifluxion processes on gentle slopes in spring and generate small landslides and mudflows on steeper segments of the basins (Corona *et al.*, 2002; Rovéra and Robert, 2005). As a consequence, the first major precipitation events in spring will usually result in flood runoff with high sediment load. In summer and early autumn, in contrast, severe storms are likely to mobilize sediments through concentrated runoff on the slopes. Similar observations were made by Regüés and Gallart (2004) for the Vallcebre basin (Spanish Pyrenees), where badland dynamics were determined by thermal and hydric periods as well: the thermal period caused the formation of regolith and sediment stocking, whereas the hydric period resulted in its erosion and runoff.

These combined processes maintain bare slopes with vegetation being generally restricted to interfluves and more stable slopes. Tree species occurring in the experimental basins are limited mostly to *Pinus sylvestris* and Austrian black pine (*P. nigra* Arn. ssp. *nigra*) and almost all trees show the typical stress symptoms and partial exposure of lateral roots (Figure 1b and 1c).

Methods

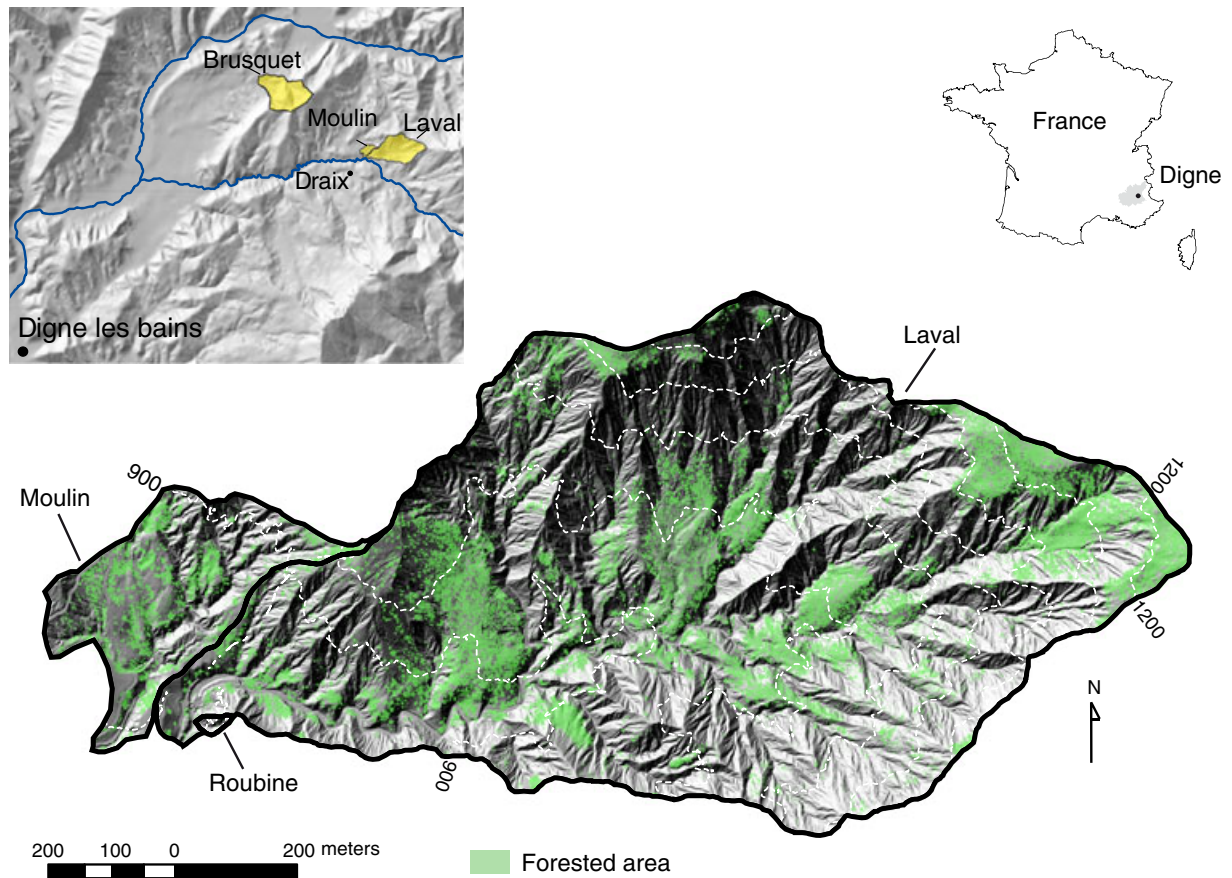
Sampling strategy and tree-ring analysis

Within this study, 48 roots from 27 different *Pinus sylvestris* trees were taken on interfluve slopes (0–15°) and on gully slopes (15–45°, Table I). Roots were sampled at a distance >50 cm from the stem to avoid possible stem-related mechanical effects on increment growth. Before cutting, the position of the exposed roots was documented in detail and data recorded on topography, altitude, aspect, root distance from tree trunk, hillside slope and slope of the specific root location. The distance from the top of the root to the ground level was measured using a 50 mm⁻¹ resolution depth gauge. All samples chosen for analysis were still living and the root tips anchored in the soil. Root samples were then cut with a handsaw into cross-sections about 2 cm thick (Figure 2a).

In the laboratory, the root sections were first prepared for macroscopic analysis (Bodoque *et al.*, 2005) and aged. As only living roots were sampled, the last growth ring corresponded to the year in which sampling took place. Dating accuracy was improved by counting growth rings on four different radii per cross-section so as to minimize the risk of misdating through the presence of false, wedging or missing rings.

In a subsequent step, cross-sections were photographed with a digital imaging system under optical microscopy (Figure 2b) and pictures analysed using the semi-automated WinCell 2009a software to quantitatively assess anatomical variations (Figure 2c) such as cell-size distribution of earlywood tracheids. Following Rubiales *et al.* (2008) and Corona *et al.* (In press), changes in tracheid cell size were determined by randomly measuring the cell lumen area of 12 tracheids per growth ring.

a



b

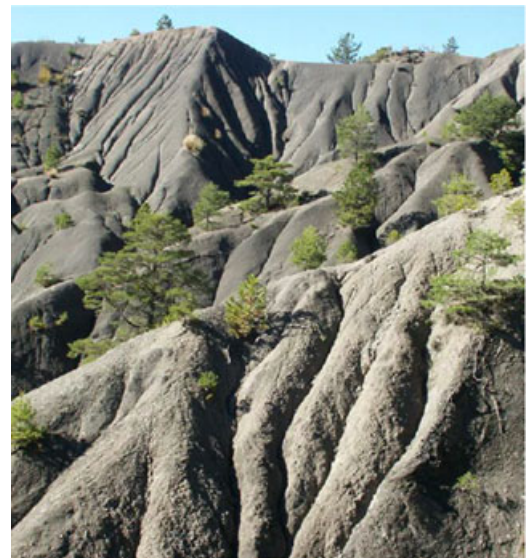


Figure 1. The Draix experimental catchment basins are located near the town of Digne-les-Bains (Alpes de Haute-Provence, France). In the Laval, Moulin and Roubine catchments, forested patches are scarce. This figure is available in colour online at wileyonlinelibrary.com/journal/espl

Quantification of erosion rates by means of exposed roots

For a highly-resolved assessment and accurate quantification of erosion rates (E_{ra}), the thickness of the eroded soil layer (E_r) and the time elapsed since exposure (NR_{ex}) need to be determined (Figure 3). In the case of continuous and progressive denudation as is the case on marly slopes, it has recently been demonstrated that a reduction of tracheid cell lumen area starts to occur as soon as the soil mantle covering

the buried root is reduced to 3 cm (Corona *et al.*, In press). For the assessment of the depth of the eroded layer (E_x), this 30 mm bias (ϵ) was subtracted from the height of the exposed root as measured in the field. Root-soil values measured in the field were also corrected to integrate the relative vertical uplift of the root axis related to the subsequent growth on both sides of the root after exposure (Gr1, Gr2; Corona *et al.*, In press) as follows:

$$E_r = E_x - (Gr1 + Gr2) + (B1 + B2)/2 + \epsilon$$

Table 1. Characteristics of exposed roots and erosion rates determined from wood-anatomical changes in exposed roots

Number of root	ID of cross-section	Topographic conditions	Age (years)	Slope (deg)	E_x (mm)	E_r (mm)	Year of exposure	Duration of exposure (NRex, years)	Erosion rate (E_{ra} , mm yr ⁻¹)
1	A	Gully slope	38	22	77	63	1996	13	7.2
1	B	Gully slope	36	22	95	77	1993	16	6.7
1	C	Gully slope	33	22	85	63	1995	14	6.6
2	A	Gully slope	28	34	68	61	1988	21	4.3
3	A	Gully slope	28	40	78	71	1991	18	5.6
4	A	Gully slope	32	41	170	160	1986	23	8.3
5	A	Gully slope	29	39	150	136	1987	22	7.6
6	A	Interfluvial slope	36	5	62	58	1991	18	4.9
7	A	Interfluvial slope	37	6	90	50	1984	25	3.2
9	A	Interfluvial slope	23	5	77	38	1992	17	5.2
9	B	Interfluvial slope	31	6	67	48	1994	15	5.2
10	A	Interfluvial slope	34	4	73	53	1993	16	5.2
11	A	Interfluvial slope	46	13	135	101	1971	38	3.4
11	B	Interfluvial slope	45	13	70	51	1995	14	5.8
12	A	Gully slope	44	38	91	65	1990	19	5.0
12	B	Gully slope	32	50	156	128	1990	19	8.3
12	C	Gully slope	33	54	165	120	1990	19	7.9
12	D	Gully slope	31	40	96	62	1993	16	5.8
12	E	Gully slope	24	50	141	109	1992	17	8.2
12	F	Gully slope	25	52	172	145	1987	22	8.0
12	G	Gully slope	17	50	95	75	1998	11	9.5
13	A	Gully slope	40	26	133	101	1987	22	6.0
13	B	Gully slope	29	25	176	150	1988	21	8.6
13	C	Gully slope	23	32	141	123	1988	21	7.3
14	A	Gully slope	60	31	52	46	1998	11	6.9
14	B	Gully slope	65	38	262	224	1965	44	5.8
14	C	Gully slope	57	41	266	236	1976	33	8.1
15	E	Gully slope	63	48	71	48	1995	14	5.6
15	F	Gully slope	61	41	108	77	1997	12	8.9
15	G	Gully slope	44	18	148	99	1973	36	3.6
15	H	Gully slope	53	27	140	105	1981	28	4.8
100	A	Gully slope	45	26	104	44	1973	36	2.1
100	B	Gully slope	46	16	83	45	1975	34	2.2
100	C	Gully slope	47	24	79	36	1973	36	1.8
100	D	Gully slope	48	28	75	35	1975	34	1.9
101	A	Gully slope	46	27	34	17	1997	12	3.9
101	B	Gully slope	20	32	68	43	1995	14	5.2
101	D	Gully slope	18	29	47	17	2000	9	4.7
101	E	Gully slope	18	31	51	22	1997	12	4.3
201	A	Interfluvial slope	18	6	32	12	1995	14	3.0
202	A	Gully slope	20	40	53	37	1999	10	6.7
203	A	Gully slope	32	43	88	77	1999	10	10.7
204	A	Gully slope	49	35	48	39	2004	5	13.8
205	E	Interfluvial slope	19	9	52	42	1997	12	6.0
206	A	Interfluvial slope	62	10	90	31	1975	34	1.8
206	B	Interfluvial slope	62	10	35	12	1993	16	2.6
207	A	Gully slope	12	47	58	34	2003	6	10.7
209	A	Gully slope	45	40	185	119	1975	34	4.4
Average			37	29	102	75		20	5.9

This equation assumes that the axial growth pressure exerted by the root is lower than the mechanical impedance of the soil, i.e. its reaction to deformation by the root. The value of E_r is finally divided by the number of rings since the year of exposure (NRex) to quantify annual erosion rates:

$$E_{ra} = E_r / \text{NRex}$$

Mapping erosion rates using slope maps derived from LiDAR data

Light detection and ranging (LiDAR) refers to the use of a laser scanner to develop high-resolution topographic data over large areas (James *et al.*, 2007). In badlands regions, LiDAR data

have been used in the past to extract thalweg networks (Thommeret *et al.*, 2010) or to derive erosion rates (Puech *et al.*, 2009; Evans and Lindsay, 2010). In this study, LiDAR data acquisition was performed in April 2007 by Sintégra (Meylan, France) using an airborne RIEGL® LMS-Q560 laser scanner. The flight height was ~600 m resulting in a footprint size of about 0.25 m. The point density was about 5 points m⁻² (Bretar *et al.*, 2009).

Erosion rates at the catchment scale were determined from high-resolution erosion maps and computed with (i) a linear regression model (ErS) involving slope (S) and dendrogeomorphic erosion rates (E_{ra}) as well as (ii) high-resolution slope maps derived from a LiDAR-generated digital elevation model (DEM) using ArcGIS Geostatistical Analyst (ESRI Corp.). The average erosion rates computed from these maps were then

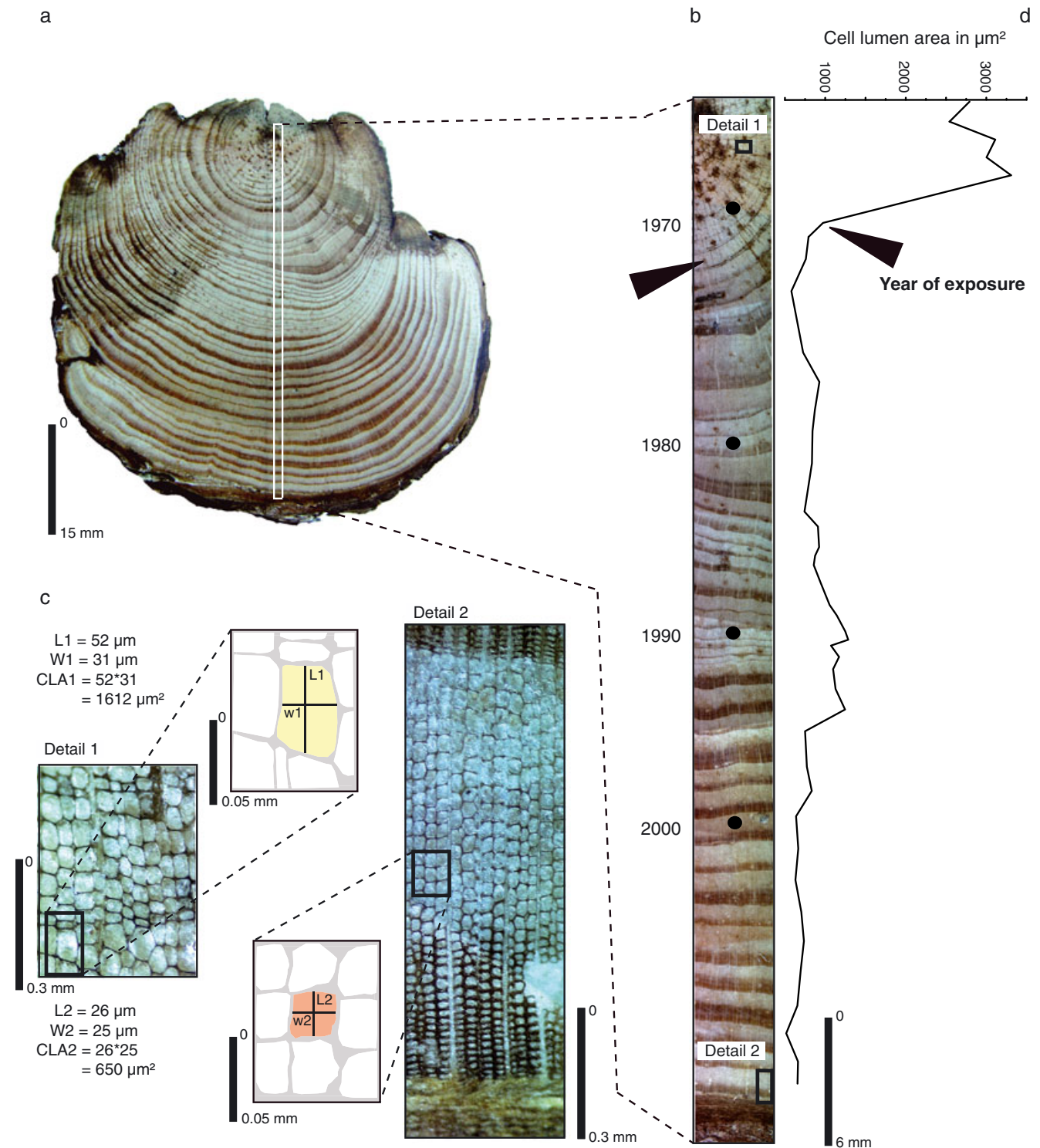


Figure 2. (A) Cross-section of exposed Scots pine (*Pinus sylvestris* L.) root R100C. (B) Detail of the cross-section after sanding with (C) cell lumen area measurements before (in yellow) and after (in red) exposure. Determination of the year of exposure (1973) was based on the sharp decrease of cell lumen area of earlywood and latewood tracheids. This figure is available in colour online at wileyonlinelibrary.com/journal/espl

compared with values derived from sedimentation rates in the traps at the outlet of the experimental catchments.

Results and Discussion

Anatomical changes in exposed roots

By way of example, Figure 2d shows the wood structure of exposed *Pinus sylvestris* root R100C for the period 1955–2007. Before 1972, the anatomical structure of this root sample is characterized by thin cell walls and large cell lumens in earlywood tracheids. From 1973 onwards, however, growth

rings exhibit a stem-like wood structure, with cell lumen areas in earlywood being reduced to ~50% and very distinct latewood tracheids becoming apparent in the root-ring series. Such abrupt cell-size reductions typically occur when a root is located in the detrital layer and at a vertical depth of ~30 mm below the soil surface. Comparable cell-size reductions were observed at different times in the past in all roots selected for analysis, indicating that all samples suffered from soil denudation and subsequent exposure between 1965 and 2004 (mean year of reaction: 1989; Table I).

The physiological interpretation of these anatomical changes can be related to the response of the coniferous vascular systems

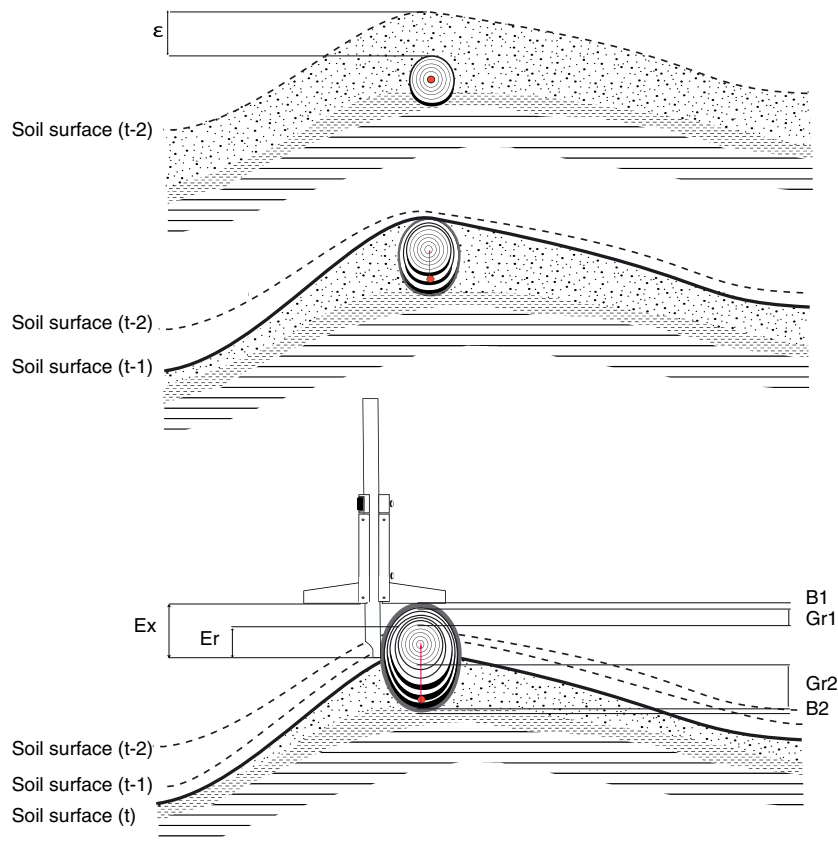


Figure 3. Schematic view of root exposure presenting the parameters used for a quantitative reconstruction of erosion rates. This figure is available in colour online at wileyonlinelibrary.com/journal/espl

to the stress that arises due to the reduced thickness of the soil layer covering the root. At the study site, soils close to surface level are composed of very porous and loose detrital layer mainly composed of angular marl fragments contained in a silty matrix and with *c*- and *b*-axes <3 cm (Oostwoud Wijdenes and Ergenzinger, 1998; Maquaire *et al.*, 2002). Roots located in these detrital layers are exposed to a larger thermal amplitude, enhanced oscillations and thus greater thermal stress. In August 2006, for instance, temperature maxima logged with a meteorological station in the Moulin Basin (Figure 4a) recorded up to 28.4 °C at –24 cm depth, 32.2 °C at –12 cm, 36.4 °C at –6 cm and 57.6 °C at –1 cm. Temperature ranges were respectively 8 °C, 13.9 °C, 20.1 °C and 47.7 °C. Similarly, in March 2006 (Figure 4b), temperature ranges were respectively 8.4 °C at –24 cm depth, 13 °C at –12 cm, 18 °C at –6 cm and 49 °C at –1 cm. At the same time, a total of 12 freeze–thaw cycles is recorded at –1 cm while such cycles are absent below this depth. Decreasing numbers of freeze–thaw cycles with depth are reported by Rovéra and Robert (2005) for the contiguous Bouinenc catchment where 23 freeze–thaw cycles were measured at a depth of –10 cm in the fragmented regolith, 61 cycles at –5 cm and 92 cycles in the loose detrital cover at –1 cm during winter 2000–2001.

In the detrital cover, roots are also exposed to higher moisture oscillations and water stress. The hourly soil moisture contents were measured at Moulin basin, on a south-facing slope, using Time Domain Reflectometry (TDR) probes. These probes are reported, for March and August 2006, in Figures 4c and 4d. In the marly bedrock (–30 cm), soil moisture exhibits slight oscillations with respective standard deviations of 0.88 and 1.85% for both months. In the loose detrital layer (–5 cm), in contrast, standard deviations are much higher (2.76% in March, 4.61% in August) and thus reveal higher moisture oscillations. Except for the aftermath of precipitation events, the hydric stress

is clearly stronger and the mean soil moisture remains lower as soon as a root approaches the soil surface. In this respect, the reduction of cell lumen area of earlywood tracheids of roots located in the loose detrital layers close to the soil surface has to be seen as a response of the vascular system of *Pinus sylvestris* to thermal and hydric stresses (Antonova and Stasova, 1993).

Erosion rates determined at the plot scale

The height of the exposed part of roots after correction for growth after exposure and bias adjustment (i.e. $\epsilon = 30$ mm) ranges between 42 and 266 mm. The year of exposure varies between 1965 and 2004 enabling the computation of multi-decadal erosion rates, with E_{ra} ranging between 1.8 and 13.8 mm yr^{–1} (average: 5.9 ± 2.6 mm yr^{–1}). These erosion rates agree with data from several erosion studies conducted in the southern French Alps using denudation measurement devices, especially stakes driven into the soil between 1998 and 2000. For instance, Robert (2000) measured erosion rates of 7 mm yr^{–1} in the Draix catchments, Rovéra *et al.* (1999) assessed erosion rates of 3–10 mm yr^{–1} (1995–1997) in the Saignon catchment (southern French Alps), Descroix (1994) and Descroix and Olivry (2002) obtained erosion rates of 4–17 mm yr^{–1} at six study sites in the Baronnies, Diois and Préalpes de Digne regions and measurement periods ranging from one to six years, Bufalo (1989) measured soil loss on bare marls in small catchments of 11.5 mm yr^{–1} between 1985 and 1988, and Lecompte *et al.* (1998) reported mean erosion rates of 7–8 mm for two catchments in the upper Méouge river basin (1990–1995).

On interfluvies, erosion rates range from 2.8 to 5.2 mm yr^{–1} (mean: 4.1 ± 1.5 mm yr^{–1}) whereas on gully slopes, values vary between 2.2 and 13.8 mm yr^{–1} (mean: 6.3 ± 2.7 mm yr^{–1}). Figure 5 displays average erosion rates obtained for 10° slope

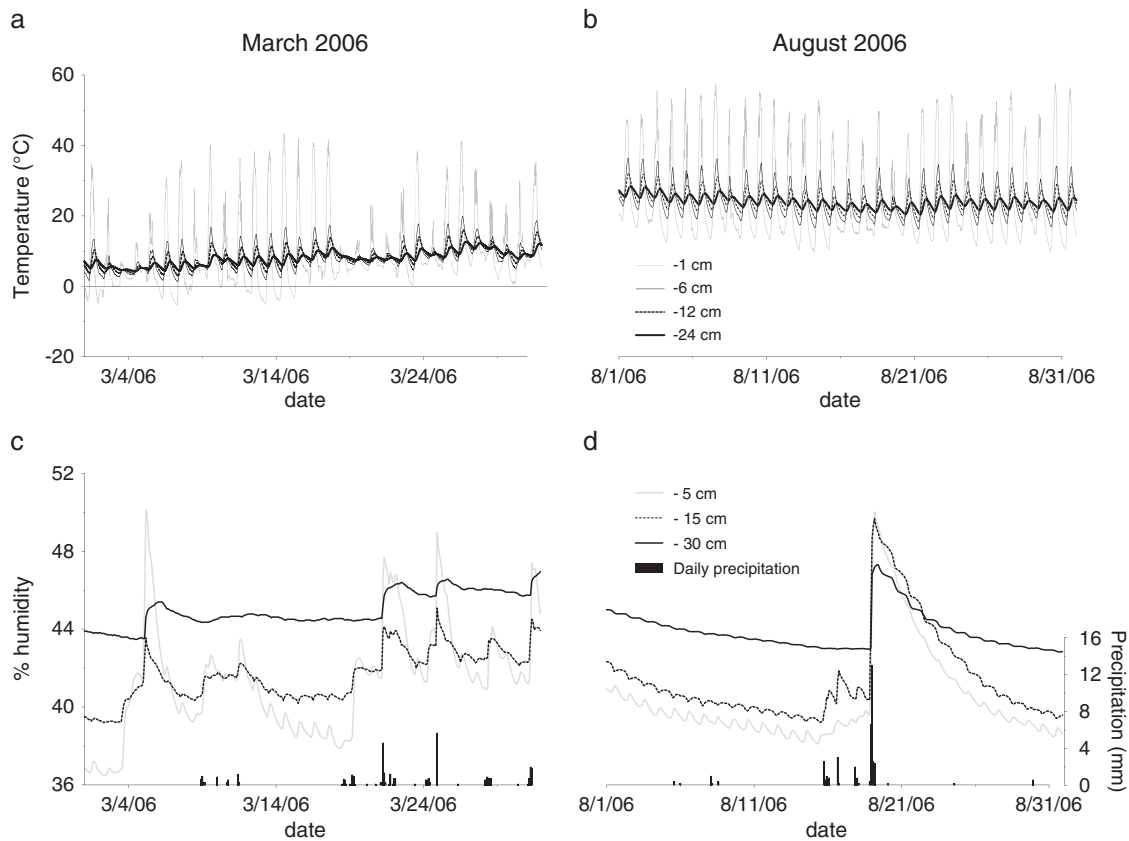


Figure 4. Hourly (a and b) soil temperature and (c and d) soil moisture data recorded between March and August 2006 at Moulin basin.

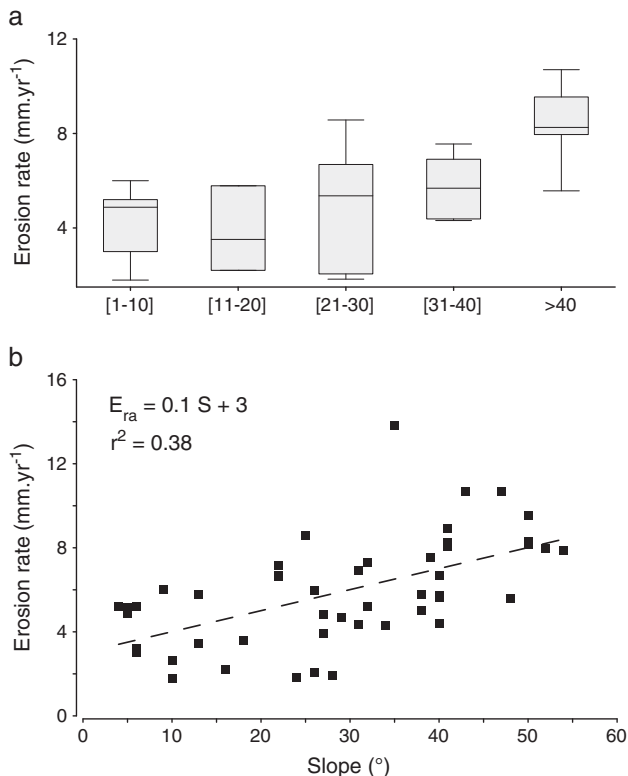


Figure 5. (a) Box plot illustrating erosion rates for different 10° slope classes and (b) linear regression model taking into account erosion rates derived from anatomical changes in roots and slopes measured in the field. The model is significant at the 0.05 level and able to predict 42% of erosion variability.

classes. Despite a high spatio-temporal variability, average erosion rates clearly exhibit a positive relationship with slope

angle. The value of E_{ra} increases from an average of 4.1 mm yr^{-1} in the class $0\text{--}10^\circ$ to 8.7 mm yr^{-1} in the class $>40^\circ$. Based on these results, a linear regression model E_r involving slope and erosion rate was derived as follows:

$$E_r = 0,1 S + 3$$

where E_r is the erosion rate measured in mm yr^{-1} , and S is the slope in degrees. The coefficient of determination (R^2) for this model is 0.42, significant at the 0.05 level, and the root mean square error (RMSE) amounts to 2.1 mm yr^{-1} . The regression model E_r clearly confirms the relationship between erosion rates and slope angle as demonstrated by several other studies (see Descroix and Olivry, 2002, for a review). On very steep bare slopes ($>45^\circ$), the regression model underestimates erosion rates, but these slopes account for a relatively small proportion of the catchment areas ($<10\%$). As only roots located on bare slopes were sampled, it seems possible that the strong variability observed for slope classes $<45^\circ$ may result from (i) the dip and structural configuration of the outcrop (Rovéra *et al.*, 1999; Descroix and Mathys, 2003) as erosion rates may be up to three times higher when slope and dip are approximately perpendicular than when they are almost parallel to the exposure of the site (Descroix and Olivry, 2002). However, (ii) exposure of the slope could also influence erosion rates as northern slopes are affected two to four times as much as southern slopes. The higher weathering and subsequent erosion rates on north-facing slopes were related to freeze–thaw and observed in the experimental basins of Draix (Descroix and Mathys, 2003) but also in the Spanish Pyrenees (Regüés and Gallart, 2004). Conversely, in the semi-arid badlands of Tabernas (southern Spain) or Basilicata (southern Italy), the influence of slope aspect on weathering and subsequent erosion rates can not be differentiated so clearly (Regüés and Gallart, 2004; Clarke and Rendell, 2006).

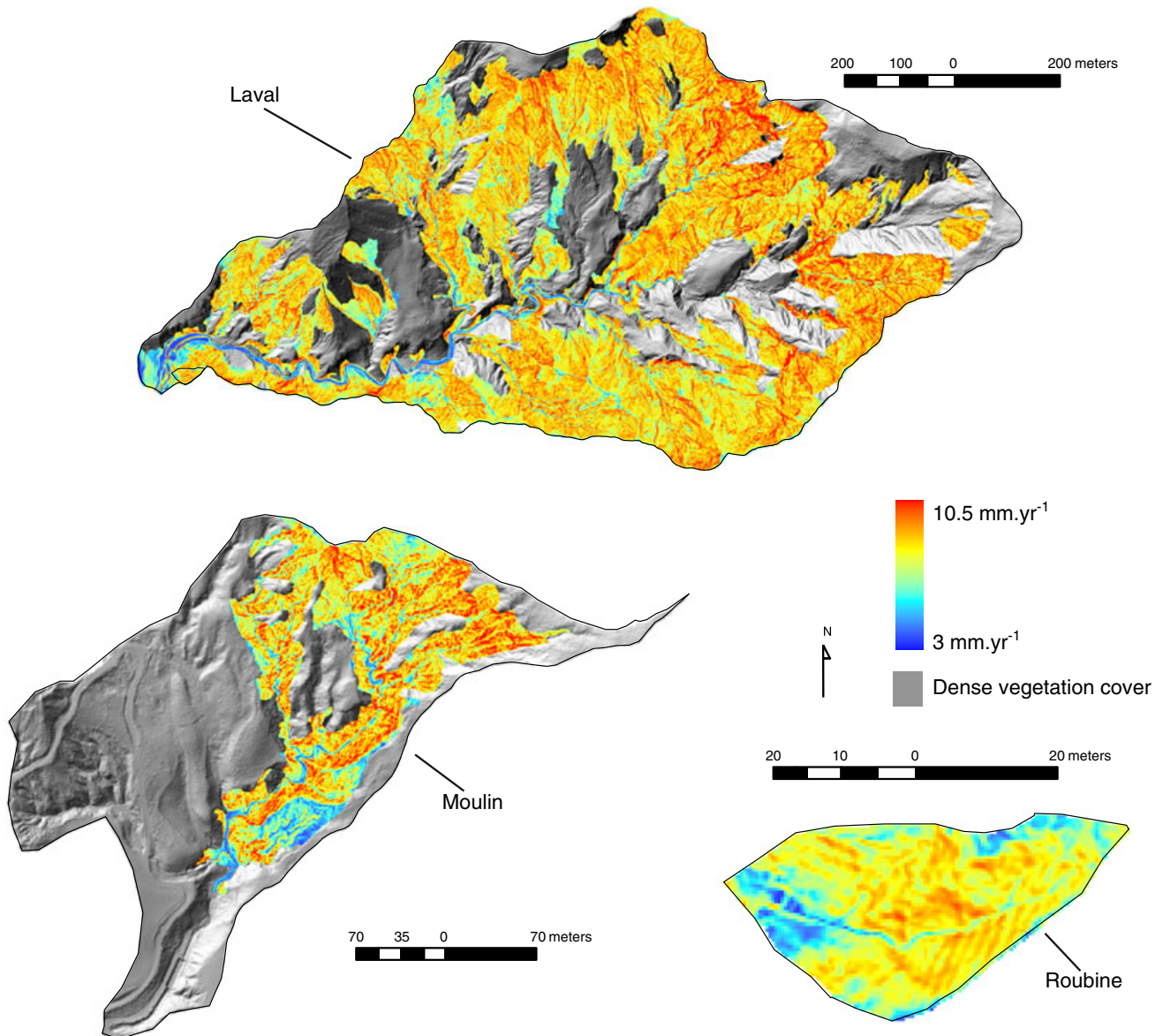


Figure 6. High-resolution erosion maps for the Laval, Moulin and Roubine catchments. Predicted erosion maps are obtained through a coupling of the linear regression model with high-resolution slope maps derived from a LiDAR-generated DEM. This figure is available in colour online at wileyonlinelibrary.com/journal/esp

Erosion rates determined at the catchment scale

The average point spacing of airborne LiDAR scanning data at the study site is in the order of 0.25 m with a cell resolution of the DEM of 0.5 m. The erosion maps resulting from the combination of the linear model with the DEM-generated slope maps are given in Figure 6 and point to erosion rates ranging from 3 to 10.5 mm yr⁻¹. The mean erosion rates computed for the Roubine, Moulin and Laval catchments are respectively 5.8, 5.2 and 6.2 mm yr⁻¹ (Table II).

These values agree with the mean annual erosion rates measured at the outlet of the experimental catchments since 1985 where values of 6.3 ± 2.5 , 4.1 ± 2.5 , and 6.4 ± 1.6 mm yr⁻¹, respectively, have been obtained for the area devoid of continuous vegetation in the Roubine, Moulin and Laval catchments (Mathys *et al.*, 1996; 1999, Mathys, 2006). The discrepancies between the two approaches may be explained by the fact that (i) the coarse material from slopes and gullies undergoes deposition, scouring and transport in the Moulin and Laval catchments whereas ablation on slopes is the dominant process in the Roubine catchment (Mathys and Klotz, 2008). In this sense, 85% of the material (in weight) is on average stocked during

floods in the traps of the Roubine catchment while only 40% is deposited in the Laval trap. The proportion of coarse material is about 42% for the Moulin watershed. In addition, differences between the model and trap measurements may also stem from (ii) the important interannual standard deviations of erosion rates at the Moulin basin ranging from 3.1 mm yr⁻¹ for the dry period 1989–1991 to 6.6 mm yr⁻¹ in 1994 as a result of an above-average frequency of rainfalls with intensities >5 mm h⁻¹ (Mathys, 2006). Finally, part of the differences is certainly due to (iii) our linear regression model which reconstructs only

Table II. Comparison of erosion rates at the catchment scale derived from high-resolution erosion maps and sedimentation in traps

Surface (ha)	Bare area (%)	Slope (%)	Erosion rate (mm yr ⁻¹ 1985-2003; Mathys, 2006)	Erosion rate (mm yr ⁻¹) (Dendrogeomorphic approach)
0.13	79	75	6.3	5.8
8	54	30	4.1	5.2
86	68	58	6.4	6.2

42% of erosion variability and underestimates erosion rates on the steepest slopes (>45°). Yet, the discrepancies of erosion variability between the local and catchment scales are smaller than those reported in previous studies using erosion pins and sedimentation dams (Sirvent *et al.* 1997, Marín and Desir, 2007). In fact, the multi-decadal erosion rates obtained for both scales minimize the scale dependency related to the temporary storage of material on the slopes in the present study.

Conclusion

This paper describes a new approach for the mapping of erosion rates in marly badlands making use of data from exposed roots of Scots pine (*Pinus sylvestris* L.). The study was successful in demonstrating that the decrease of mean lumen area of earlywood tracheids is a response of the vascular system to increasing temperatures and drought stress which occur in the upper detrital loose layer and as soon as the root approaches the soil surface. At the plot scale, a comparison with data from several studies using denudation measurement devices – in particular stakes driven into the soil – demonstrates the reliability of erosion rates determined from anatomical changes in exposed roots at the decadal scale.

A linear regression model using slope as an independent variable is able to predict 42% of erosion variability. When coupled to high-resolution slope maps derived from a LiDAR-generated DEM, this model data can be used to generate high-resolution erosion maps for catchments affected by erosion. At the catchment scale, predicted mean erosion rates obtained from dendrogeomorphic and regression model data do not differ significantly from sediment yield measured in traps at the outlet of the basins.

The mapping of erosion rates for entire sub-catchments is very innovative and represents considerable progress in the field of erosion assessment. This approach could be replicated for the establishment of records in undocumented Mediterranean badland areas and more generally in regions of continuous erosion with distinct seasons where historical data are scarce or absent. It should be used for an accurate localization of the main sediment sources, an improved and sustainable location of storage lakes, and for an effective planning of rehabilitation measures.

Acknowledgments—This research has been supported by the PARAMOUNT programme, 'ImProved Accessibility, Reliability and security of Alpine transport infrastructure related to MOUNTainous hazards in a changing climate', funded by the Alpine Space Programme, European Territorial Cooperation, 2007–2013. It has also been supported by the DENDROGLISS programme, funded by the MAIF foundation and the Cemagref as well as by the EU-FP7 project ACQWA (project no. GOCE-20290). The authors would like to acknowledge N. Mathys and the members of GIS Draix for granting access to databases and address warm thanks to E. Arbellay for her essential contribution on anatomical analysis. The authors are most grateful to F. Kirkby and to two journal reviewers whose insightful comments helped them to improve an earlier version of the paper.

References

- Antoine P, Giraud D, Meunier M, Van Asch T. 1995. Geological and geotechnical properties of the 'Terres Noires' in southeastern France: weathering, erosion, solid transport and instability. *Engineering Geology* **40**: 223–234. DOI: 10.1016/0013-7952(95)00053-4
- Antonova GF, Stasova VV. 1993. Effects of environmental factors on wood formation in Scots pine stems. *Trees* **7**: 214–219.
- Bretar F, Chauve A, Bailly JS, Mallet C, Jacome A. 2009. Terrain surfaces and 3-D landcover classification from small footprint full-waveform lidar data: application to badlands. *Hydrology and Earth System Sciences* **13**: 1531–1545.
- Bodoque JM, Díez-Herrero A, Martín-Duque JF, Rubiales JM, Godfrey A, Pedraza J, Carrasco RM, Sanz MA. 2005. Sheet erosion rates determined by using dendrogeomorphological analysis of exposed tree roots: two examples from Central Spain. *Catena* **64**: 81–102. DOI: 10.1016/j.catena.2005.08.002
- Bouma NA, Imeson AC. 2000. Investigation of relationships between measured field indicators and erosion processes on badland surfaces at Peter, Spain. *Catena* **40**: 147–171.
- Bufalo M. 1989. *L'érosion des terres noires dans la région du Buëch (Hautes-Alpes, France)*, PhD Thesis, Aix-Marseille III, 230 pp.
- Clarke ML, Rendell HM. 2006. Process–form relationships in southern Italian badlands: erosion rates and implications for landform evolution. *Earth Surface Processes and Landforms* **31**: 15–29.
- Clarke ML, Rendell HM. 2010. Climate-driven decrease in erosion in extant Mediterranean badlands. *Earth Surface Processes and Landforms* **35**(11): 1251–1371. DOI: 10.1002/esp.1967.
- Corona C, Robert Y, Rovera G. 2002. Suivi de l'érosion et modélisation des vitesses de déplacement des sédiments sur versants marneux très dégradés. Application sur les badlands de Draix grâce au topomicromètre laser photographique. In *Proceedings of the Symposium 'Geomorphology: From Expert Opinion to Modelling'*, Delahaye D, Levoy F, Maquaire O (eds), CERG Editions, Strasbourg.
- Corona C, Lopez Saez J, Rovéra G, Astrade L, Stoffel M, Berger F. 2010. Validation d'une méthode de quantification des vitesses d'érosion sur marnes par dendrogeomorphologie (Draix, Alpes de Haute-Provence). *Géomorphologie: relief, processus, environnement* **1**: 83–94.
- Corona C, Lopez Saez J, Rovéra G, Stoffel M, Astrade L, Berger F. 2011. Highly-resolved, quantitative reconstruction of erosion rates based on anatomical changes in exposed roots (Draix, Alpes de Haute-Provence) – critical review of existing approaches and independent quality control of results. *Geomorphology* **125**: 433–444. DOI: 10.1016/j.geomorph.2010.10.030
- Delannoy JJ, Rovéra G. 1996. L'érosion dans les Alpes occidentales: contribution à un bilan des mesures et des méthodes. *Revue de Géographie Alpine* **84**: 87–101.
- Descroix L. 1994. *L'érosion actuelle dans la partie occidentale des Alpes du Sud*, PhD Thesis, Université Lumière Lyon II, 290 pp.
- Descroix L, Olivry JC. 2002. Spatial and temporal factors of hydric erosion in black marls badlands of the French southern Alps. *Journal of Hydrological Sciences* **47**(2): 227–242.
- Descroix L, Mathys N. 2003. Processes, spatio-temporal factors and measurements of current erosion in the French southern Alps: a review. *Earth Surface Processes and Landforms* **28**: 993–1011. DOI: 10.1002/esp.514
- Evans M, Lindsay J. 2010. High resolution quantification of gully erosion in upland peatlands at the landscape scale. *Earth Surface Processes and Landforms* **35**: 876–886.
- James LA, Watson DG, Hansen WF. 2007. Using LiDAR data to map gullies and headwater streams under forest canopy: South Carolina, USA. *Catena* **71**: 132–144.
- Kuhn NJ, Yair A. 2004. Spatial distribution of surface conditions and runoff generation in small arid watersheds, Zin Valley Badlands, Israel. *Geomorphology* **57**: 183–200. DOI: 10.1016/S0169-555X(03)00102-8
- LaMarche VC. 1968. *Rates of Slope Degradation as Determined from Botanical Evidence White Mountains California*, United States Geological Survey Professional Paper 352-I. US Geological Survey: Reston, VA.
- Lasanta T, Arnáez J, Oserín M, Ortigosa LM. 2001. Marginal lands and erosion in terraced fields in the Mediterranean mountains: a case study in the Camero Viejo (northwestern Iberian system, Spain). *Mountain Research and Development* **21**: 69–76.
- Lecompte M, Lhénaff R, Marre A. 1998. Huit ans de mesure du avinement des marnes dans les Baronnies méridionales (Préalpes françaises du Sud). *Géomorphologie: relief, processus, environnement* **4**: 351–374.
- Maquaire O, Ritzenthaler A, Fabre D, Ambroise B, Thierry Y, Truchet E, Malet JP, Monnet J. 2002. Caractérisation des profils de formations superficielles par pénétrométrie dynamique à énergie variable :

- application aux marnes noires de Draix (Alpes-de-Haute-Provence, France). *Comptes Rendus Geoscience* **334**: 835–841. DOI. 10.1016/S1631-0713(02)01788-1
- Marín C, Desir G. 2007. Factors controlling the erosion rates in a semi-arid zone (Bardenas Reales, NE Spain). *Catena* **71**: 31–40.
- Mathys N. 2006. *Analyse et modélisation à différentes échelles des mécanismes d'érosion et de transport solides. Cas des petits bassins versants de montagne sur marnes (Draix, Alpes-de-Haute-provence)*, PhD Thesis, Grenoble.
- Mathys N, Brochot S, Meunier M. 1996. L'érosion des Terres Noires dans les Alpes du sud : contribution à l'estimation des valeurs annuelles moyennes (bassins versants expérimentaux de Draix, Alpes de Haute Provence, France). *Revue de géographie alpine* **84**: 17–27.
- Mathys N, Bergougnoux L, Olivier JE. 1999. Sediment measurements in small mountainous badlands catchments: experiments and results from experimental catchments of Draix, (Alpes de Haute-Provence), France. In *ASCE 1999 International Water Resource Engineering Conference. Water Resources into the New Millenium: Past Accomplishments, New Challenges*, Seattle, WA, 8–12 August; 10.
- Mathys N, Brochot, S, Meunier M, Richard D. 2003. Erosion quantification in the small marly experimental catchments of Draix (Alpes-de-Haute-Provence, France). Calibration of the ETC rainfall runoff-erosion model. *Catena* **50**: 527–548. DOI. 10.1016/S0341-8162(02)00122-4
- Mathys N, Poesen J. 2005. Ravinement en montagne: processus, mesures, modélisation, régionalisation. *Géomorphologie: relief, processus, environnement* **1**: 3–6.
- Mathys N, Klotz S. 2008. Draix: a field laboratory for research on hydrology and erosion in mountain. In *Proceedings of the 4th Canadian Conference on Geohazards: From Causes to Management*, Presse de l'Université Laval, Québec, 594 pp.
- Oostwoud Wijdenes DJ, Ergenzinger P. 1998. Erosion and sediment transport on steep marly hillslopes, Draix, Haute-Provence, France: an experimental field study. *Catena* **33**: 179–200. DOI. 10.1016/S0341-8162(98)00076-9
- Puech C, Thommeret N, Kaiser B, Bailly JS, Jacome A, Rey F, Mathys N. 2009. MNT à très haute résolution dans les modelés fortement disséqués: des données aux tests d'application. *Géomorphologie: relief, processus, environnement* **2**: 141–152.
- Regüés D, Gallart F. 2004. Seasonal patterns of runoff and erosion responses to simulated rainfall in a badland area in Mediterranean mountain conditions (Vallcebre, southeastern Pyrenees). *Earth Surface Processes and Landforms* **29**: 755–767.
- Richard D, Mathys N. 1999. Historique, contexte technique et scientifique des BVRE de Draix. Caractéristiques, données disponibles et principaux résultats acquis au cours de dix ans de suivi. *Actes du colloque 'Les bassins versants expérimentaux de Draix, laboratoire d'étude de l'érosion en montagne'*, Draix, Le Brusquet, Digne, 22–24 October 1997. Cemagref: Grenoble; 11–28.
- Robert Y. 2000. *Modélisation et techniques de mesure de l'érosion dans les bad-lands marneux des Alpes du Sud. Approche à l'échelle de la ravine dans les bassins-versants de Draix (Alpes Françaises du Sud)*, MSc Thesis, Université de Grenoble, 135 pp.
- Rovéra G, Robert Y, Coubat M, Nedjai R. 1999. Erosion et stades biorhexistrasiques dans les ravines du Saignon (Alpes de Provence), essai de modélisation statistique des vitesses d'érosion sur marnes, Etudes de Géographie Physique. In *Actes du colloque 'La montagne méditerranéenne'*, 8–10 October 1998, Aix-en-Provence; 109–115.
- Rovéra G, Robert Y. 2005. Conditions climatiques hivernales et processus d'érosion périglaciaires dans les badlands marneux de Draix (800 m, Alpes du Sud, France). *Géographie Physique et Quaternaire* **59**: 31–48.
- Rubiales JM, Bodoque JM, Ballesteros JA, Díez-Herrero A. 2008. Response of *Pinus sylvestris* roots to sheet-erosion exposure: an anatomical approach. *Natural Hazards and Earth System Sciences* **8**: 223–231.
- Sirvent J, Desir G, Gutierrez M, Sancho C, Benito G. 1997. Erosion rates in badland areas recorded by collectors, erosion pins and profilometer techniques (Ebro Basin, NE-Spain). *Geomorphology* **18**: 61–75. DOI. 10.1016/S0169-555X(96)00023-2
- Stoffel M, Bollschweiler M. 2008. *Tree-ring analysis in natural hazards research – an overview*. *Natural Hazards and Earth System Sciences* **8**: 187–202.
- Stoffel M, Bollschweiler M, Butler DR, Luckman BH. 2010. *Tree Rings and Natural Hazards – A State-of-the-art*. Springer: Berlin; 505 pp.
- Thommeret N, Bailly JS, Puech C. 2010. Robust extraction of thalwegs network from DTM: application on badlands. *Hydrology and Earth System Sciences Discussion* **7**: 879–905.
- Tribak A, El Garouani A, Abahrour M. 2009. Évaluation quantitative de l'érosion hydrique sur les terrains marneux du PréRif oriental (Maroc): cas du sous-bassin de l'oued Tlata. *Sécheresse* **20**: 333–337.
- Verstraeten G, Bazzoffi P, Lajczak A, Radoane M, Rey F, Poesen J, de Vente J. 2006. Reservoir and pond sedimentation in Europe. In *Soil Erosion in Europe*, Boardman J, Poesen J (eds). Wiley: Chichester; 759–774.
- Walling DE. 1988. Measuring sediment yield from river basins. In *Soil Erosion Research Methods*, Lal R (ed.). Soil and Water Conservation Society: Ankeny, IA; 39–73.